Asian Journal of Chemistry; Vol. 31, No. 8 (2019), 1825-1829

ASIAN JOURNAL OF CHEMISTRY

https://doi.org/10.14233/ajchem.2019.22066

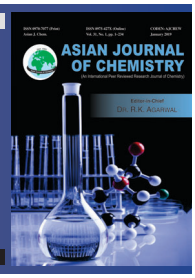

Effect of Precursors on Structural and Optical Properties of Sol-Gel Synthesized ZnO Nanopowders

A. VANAJA[1,*], JAISON JEEVANANDAM[2] and M. SURESH[3]

[1]Department of Physics, Amrita Sai Institute of Science & Technology, Paritala-521180, India
[2]Department of Chemical Engineering, Faculty of Engineering and Sciences, Curtin University, Miri, Sarawak 98009, Malaysia
[3]Post Graduate and Research Department of Advanced Zoology & Biotechnology, Loyola College (Autonomous), Chennai-600034, India

*Corresponding author: E-mail: vanajatunuguntla@yahoo.com

Received: 12 March 2019; *Accepted*: 15 April 2019; *Published online*: 28 June 2019; AJC-19460

The present work aims at evaluating the outcome of zinc precursors on the crystal structure, shape, surface and optical properties of ZnO nanopowders. Zinc oxide nanopowders are fabricated *via* simple, cost-effective, low-temperature, the sol-gel method using different zinc precursors such as zinc nitrate and zinc chloride. The structural properties of the obtained ZnO nanopowders are studied using X-ray diffraction spectra and their morphology from SEM micrographs. Further, Fourier transform infrared spectra reveals the existence of functional groups that supports the formation of zinc oxide. Moreover, optical absorption and emission of ZnO nanopowders were evaluate during ultraviolet-visible and photoluminescence spectra. The results of this study revealed that the precursor is significant in altering the crystallite size, shape, optical absorption and emission entities of nanopowders. In addition, the role of zinc precursors to fabricate nanopowders that is suitable for various optoelectronic device applications were also discussed.

Keywords: ZnO nanopowders, Crystallite size, Morphology, Opto-electronic devices.

INTRODUCTION

In the past, semiconductor nanoparticles gained importance innumerous industrial, biomedical and electronic applications due to their extremely large surface area with quantum size effect [1]. The synthesis and characterization of semiconductor nanoparticles are crucial in determining their exclusive properties and applications [2]. In recent times, these nanoparticles are successfully utilized in various commercial products including solar cells, catalysts, light-emitting diodes and opto-electronic devices [3]. Metal oxide nanoparticles are unique semiconductors that possess enhanced large surface area, chemical stability, biocompatibility, improved electrical characteristics, elevated optical absorption with less toxicity, compared to other nano-sized semiconductors. Further, these nanoparticles are utilized as building blocks for optoelectronic and electronic devices [4]. Among metal oxide nanoparticles, ZnO is extensively used in several applications due to their direct, extensive band gap of 3.37 eV, elevated exciton binding energy of 60 meV, eclectic transparency, increased electron mobility, robust room temperature luminescence, enhanced chemical stability, improved flexibility and absorption during fabrication. These properties of ZnO nanoparticles have attracted researchers to fabricate optoelectronic devices and luminescent materials [5].

Several studies reported chemical approaches for the fabrication of ZnO nanopowders with different sizes, morphologies and surface properties [6-8]. In recent times, coprecipitation, microemulsion, laser ablation, solid state reaction method, melt mixing and ball milling is used to synthesize ZnO nanopowders for desired applications [9-11]. However, utilization of toxic chemicals and tedious synthesis procedures are considered as challenges to use these approaches for down streaming processes [12-15]. Thus, the present study focuses on utilizing simple sol-gel procedure with commonly available, less toxic and cost-effective zinc precursors to fabricate ZnO nanopowders for optoelectronic device applications [16]. Further, literatures suggested that the synthesis parameters such as concentration and type of precursor, reaction time, pH variations, temperature, concentration of reagents and catalysts, phase transition in sol-gel process and calcination has ability to influence the size

distribution of ZnO nanopowders. The alterations in size distribution and morphology of ZnO nanopowders due to synthesis parameters eventually leads to the adjustments in the electrical, optical and magnetic entities of nanoparticles for suitable applications [17-19]. Hence, the present study also focuses on identi-fying the outcome of distinct zinc precursors in controlling the ZnO crystallite size, thereby, altering the size and morphol-ogy of nanopowders *via* sol-gel method to be beneficial in opto-electronic device fabrications.

EXPERIMENTAL

Chemicals such as zinc chloride with molecular weight of 136.2 g/mol and 98 % purity and $Zn(NO_3)_2 \cdot 6H_2O$ with molecular weight of 189.3 g/mol and 98 % purity are procured from Sigma-Aldrich (Singapore) and used as precursors. Other chemicals such as sodium hydroxide with molecular weight of 39.9 g/mol and 98 % purity as gelling agent and 99 % pure ethanol with molecular weight of 46.07 g/mol as solvent were purchased from Alfa-Aesar (India). All the chemicals utilized in the current study are in analytical grade and no further purification processes are required before experiment.

Fabrication of ZnO nanopowders: Initially, 0.2 M of zinc nitrate was dissolved in aqueous ethanol solution under constant stirring for 2 h in a magnetic stirrer. Simultaneously, 0.2 M of NaOH was dissolved in aqueous ethanol. The aqueous solution of NaOH was mixed slowly with an aqueous zinc nitrate solution for 10 min under constant stirring for 350 rpm. Later, the transparent solution with precursor and gelling agent are allowed for constant stirring for 3 h, until the solution turns into white gel. In this procedure, the reaction temperature was maintained at 70 ºC, constantly throughout the experiment. The obtained white gels were sealed in a beaker and left undisturbed for over-night (12 h) for complete settlement of particles. The white gel was then cleaned with deionized water and ethanol for three times to eliminate unreacted impurities. The washed sample was dried in an oven at 70 ºC for 24 h. The drying process leads to white powders which were subjected to further systematic characterizations to evaluate the formation of ZnO nanopowders. A similar procedure was used to synthesize ZnO nanopowders from zinc chloride. Finally, both the samples were analyzed to evaluate the outcome of zinc precursors in altering the properties of ZnO nanopowders.

The synthesized nanopowders were labeled as **sample A**: ZnO nanopowders synthesized by zinc chloride as precursors, and **sample B**: ZnO nanopowders synthesized by zinc nitrate as precursors

X-ray diffraction: The XRD pattern of powders was recorded *via* powder X-ray diffractometer (XRD-SMART lab-Rikagu, Japan) under the conditions such as secondary CuKα monochromatic radiation of wavelength λ = 0.1541 nm at 40 kv/50 mA in the scan range of 2θ = 20 to 90º. The powder samples are mounted on a glass slide and the crystallographic properties including crystallite size and lattice strain are determined from XRD pattern.

Scanning electron microscopy (SEM): SEM micrographs of nanopowders are observed at different magnifications using field emission scanning electron microscope (FESEM-SUPRA 55-CARL ZEISS, Germany). A drop of nanopowder samples were dissolved in methanol and were mounted over a copper grid. The SEM micrographs are highly beneficial in studying the morphology of the nanopowders.

Fourier transform infrared (FTIR): FTIR spectra of sol-gel samples were obtained from FT-Raman Spectrophotometer 5000-50 cm^{-1} (Bruker RFS). The vibrational peaks in the FTIR spectra represent the functional group present in the sample.

UV-visible absorption: The optical properties of ZnO nanopowders are determined from Varian Cary 5E UV-VIS NIR. The spectra contain information about various absorption peaks present in both ultraviolet and visible region. The powder was methanol dissolved and the colloidal nanopowders are placed in a quartz cuvette with a 1 cm path length to analyze the optical property of samples.

Photoluminescence: The photoluminescence spectra of the samples are obtained *via* a spectrofluorometer (F-2500 FL Spectrophotometer, Hitachi). The powder was dissolved in ethanol for recording spectra and the peaks help to identify the luminescence emission and the behaviour of the samples in UV and visible light region.

RESULTS AND DISCUSSION

Crystallinity of ZnO nanopowders: Crystallographic properties of nanopowders including composition, lattice parameter, crystal structure, dislocation density and residual stress are obtained from XRD spectra. Figs. 1 and 2 represent the XRD spectrum of ZnO nanopowders that are fabricated using zinc chloride (sample A) and zinc nitrate (sample B) as precursors, respectively. XRD patterns of both the samples revealed the formation of typical wurtzite ZnO structure (hexagonal phase,

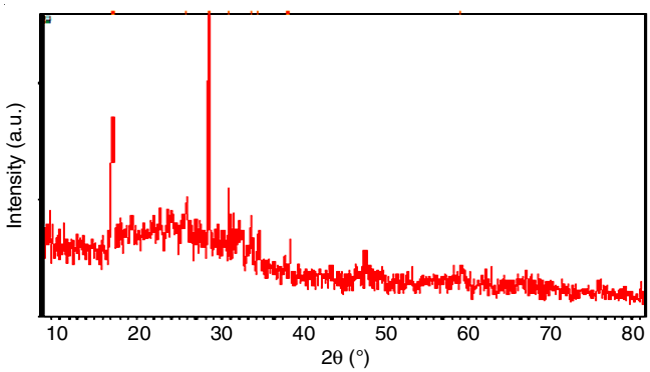

Fig. 1. XRD spectrum of sample A

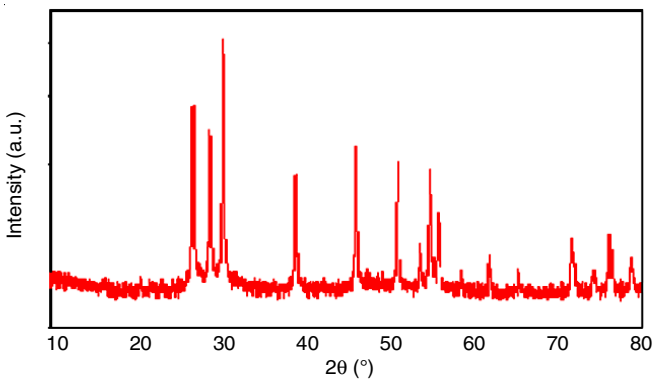

Fig. 2. XRD spectrum of sample B

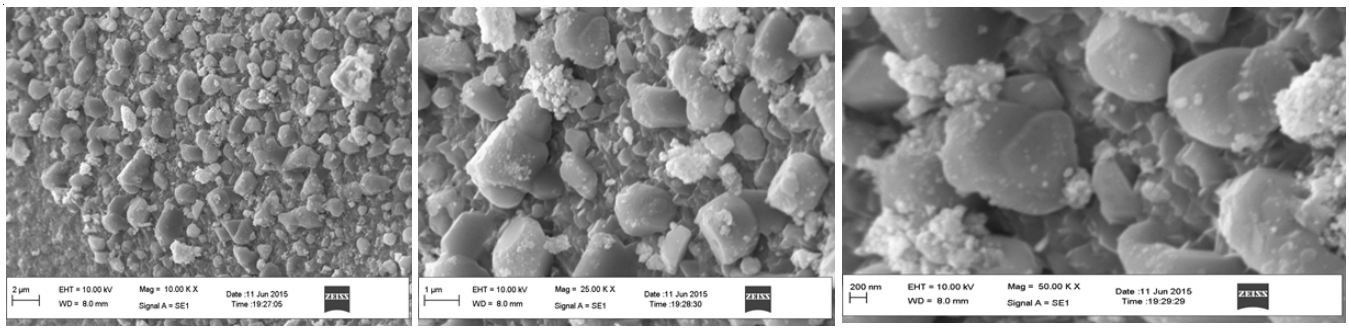

Fig. 3. SEM micrographs of sample A

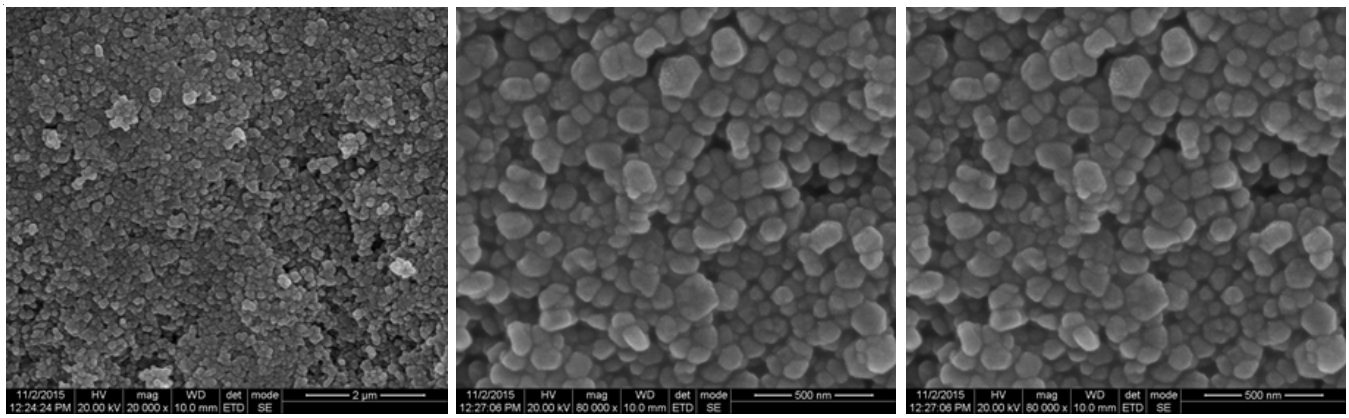

Fig. 4. SEM micrographs of sample B

space group $P6_3mc$ and JCPDS no. 36-1451). All the peaks in both the samples are exactly matching with JCDPS file that represents wurtzite ZnO with certain increments in the peak intensities, peak shifts and presence of peaks due to presence of impurities. The average nanopowder crystallite size was attained from the peaks of XRD *via* Scherer′s equation of $D = 0.9\,\lambda/\beta\cos\theta$, where λ is the incident XRD beam wavelength, θ is the angle of Bragg′s diffraction and β is the full width-half maximum of XRD peaks in radians. The crystallite size and lattice strain are calculated to be 61.26 and 0.0024 nm for sample A and 37.87 nm and 0.0030 for sample B, respectively. The results revealed that a high crystalline ZnO nanopowders are formed, when zinc nitrate is used as precursor compared to zinc chloride [20,21].

Morphology of ZnO nanopowders: Figs. 3 and 4 represent the SEM micrographs of nanopowders that are viewed at various magnifications. The micrographs proved the nanosized ZnO formation. The correlation of XRD spectra and the SEM images demonstrated that different zinc precursors influence the morphology of ZnO nanopowders. Further, the SEM images of sample A demonstrate the formation of particles with different morphologies such as rectangular, triangular and cube-like and the presence of spherical particles in sample B. Furthermore, the agglomeration of nanoparticles is less in both the samples which revealed their monodispersity property [22].

FTIR analysis: Figs. 5 and 6 represents the FTIR spectra of sample A and B, respectively, are obtained at room temperature in the wavenumber between 4000-400 cm^{-1}. Peaks attributed to water molecules are observed around 3400 cm^{-1} in the form H and OH. Strong peaks appeared around 1600 and 1300 cm^{-1} show the existence of C=O and C-O stretching

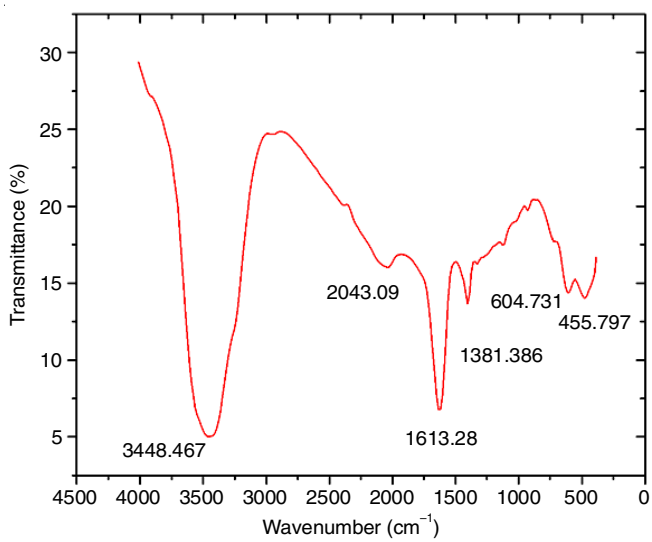

Fig. 5. FTIR spectra of sample A

vibrations of carbonyl group. The peak at 2043.09 cm^{-1} present in sample A and two peaks at 2406 and 2096 cm^{-1} present in sample B are due to the atmospheric CO_2 that interacted with the sample. FT-IR spectra exhibited Zn-O vibrational band at 450 cm^{-1}, which confirms the existence of zinc oxide in both the samples [23].

Optical properties of ZnO nanopowders: Absorption of scattered visible (390 nm to 800 nm) and UV-light (190 nm to 390 nm) and its evaluation *via* spectroscopy is a technique to characterize the optical properties of samples. The spectrum of absorption will reveal various absorption bands that represent the structural groups within the molecule.

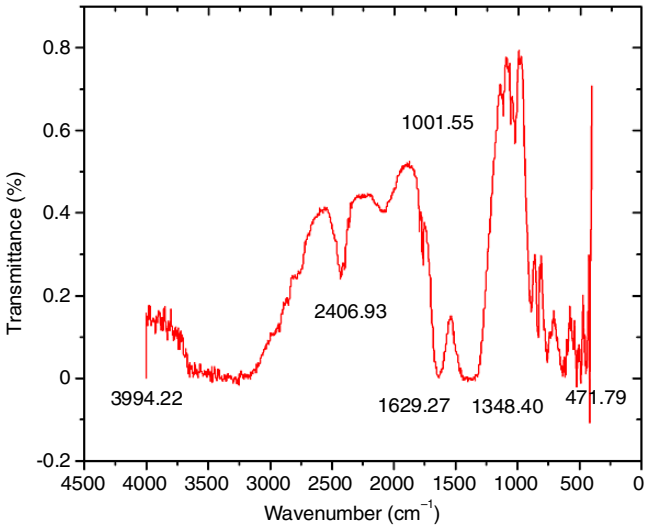

Fig. 6. FTIR spectra of sample B

Figs. 7 and 8 represented the spectra of optical absorption by sample A and B, respectively. Absorption characteristics of nanopowders are demonstrated from these spectral analyses. The absorption peak of excitons are detected around 230 nm, which is present at 388 nm that are below the wavelength of bulk ZnO band gap (E_g = 3.2 eV). From the spectral analysis, it is also demonstrated that ZnO exhibited a sharp absorption peak, which specifies the monodispersity of samples. It is evident that the edge of absorption peaks shifts systematically towards the lower wavelength or elevated energy, depending on the nanoparticle size that are fabricated with different precursors. This noticeable and efficient shift in the edge of absorption peaks is due to the nanosized quantum effect of ZnO powders [24].

Photoluminescence: Figs. 9 and 10 represent the photoluminescence spectra of sample A and B, respectively, which are recorded over the wavelength range 350-600 nm. Three unique peaks of emission were detected in the photoluminescence spectra. The emission peak around 360 nm is related to the radiative electrons and photogenerated holes recombination. In addition, the two peaks are noticed around 490 and

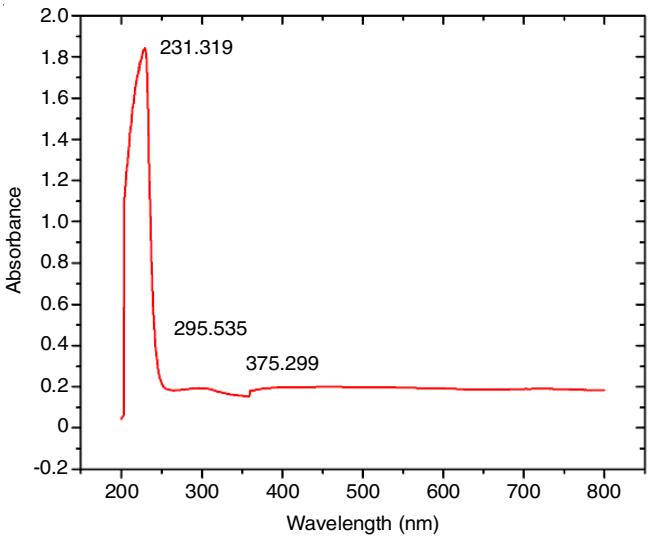

Fig. 7. Optical absorption spectra of sample A

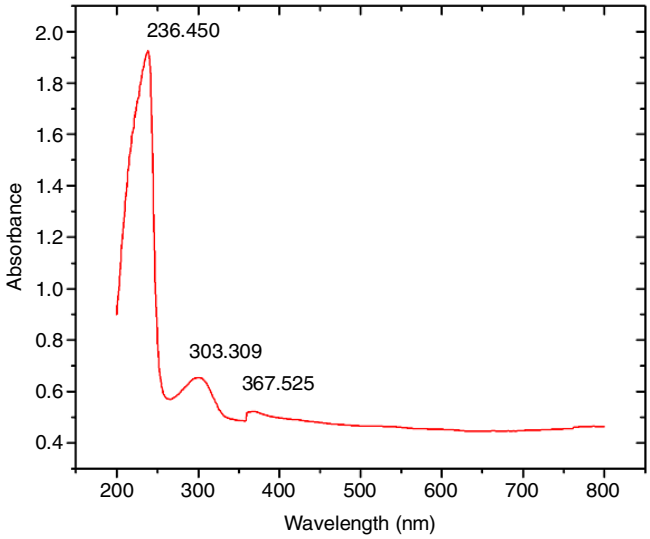

Fig. 8. Optical absorption spectra of sample B

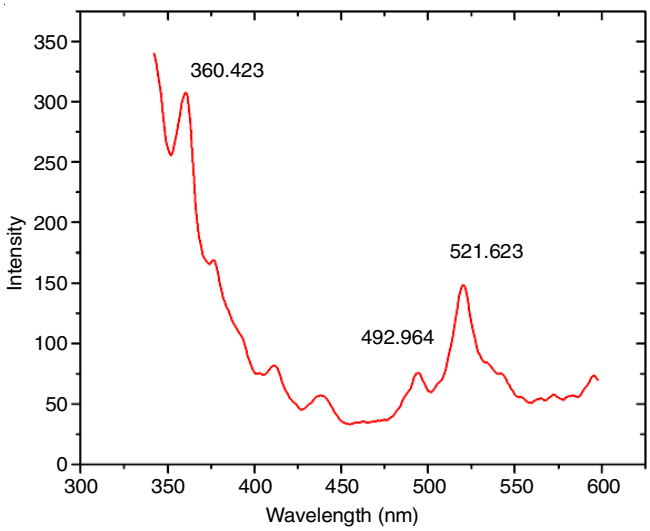

Fig. 9. Photoluminescence spectra of sample A

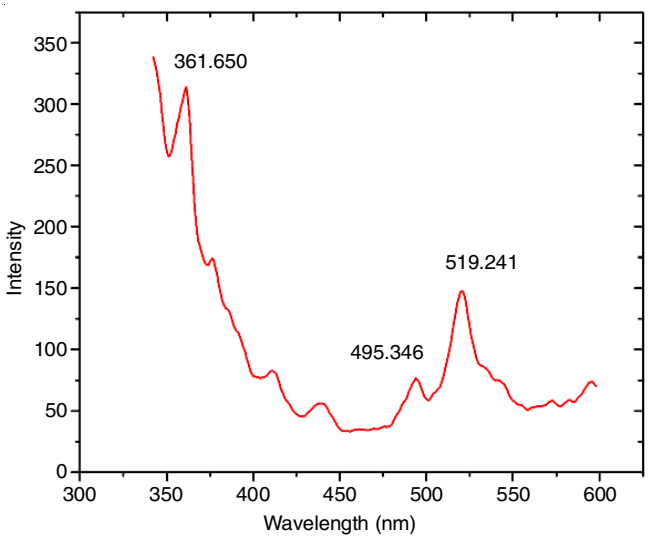

Fig. 10. Photoluminescence spectra of sample B

500 nm in the visible region. Emissions spectra in the visible light region may emerge due to numerous defect levels, such as doping, presence of interstitial zinc ion and vacancies formed

due to the ionization process of oxygen. However, present study doesn't focus on the dopants and thus, the impurities in the crystal structure are not an influential factor that elevates luminescence. From photoluminescence spectra, it is evident that no significant alterations in the emission peak position were observed, due to the influence of different zinc precursors. Small alterations in the intensities of trap-state emissions are also detected in both samples A and B synthesized with different zinc precursors [25].

Conclusion

Zinc oxide nanopowders are synthesized *via* sol-gel approach at room temperature using different zinc precursors, which are analyzed using XRD, SEM, FTIR spectroscopy, UV-visible optical absorption and photoluminescence spectroscopy. Influence of zinc precursors on the crystal structure, shape and optical entities of ZnO nanopowders is analyzed. XRD revealed that powders with different zinc precursors contribute to the formation of ZnO nanopowders with hexagonal wurtzite structure and different crystalline sizes of 61.26 nm (sample A) and 36.87 nm (sample B). The morphology of nanopowders is nearly spherical in sample B, whereas different morphologies are present in sample A. FTIR spectral analysis authenticates the existence of Zn-O in both the samples along with carbonyl functional groups. The optical studies showed that the nanopowders have a strong absorption band in the UV region and emit visible light at high intensity. Thus, it is proved from the present study that zinc precursors are significant in determining the properties of ZnO nanopowders and zinc nitrate yields smaller as well monodispersed nanopowders that are beneficial for the fabrication of optoelectronic devices.

CONFLICT OF INTEREST

The authors declare that there is no conflict of interests regarding the publication of this article.

REFERENCES

1. S. Ali, I. Khan, S.A. Khan, M. Sohail, R. Ahmed, A. Rehman, M.S. Ur Ansari and M.A. Morsy, *J. Electroanal. Chem.*, **795**, 17 (2017); https://doi.org/10.1016/j.jelechem.2017.04.040.
2. H.-S. Chen, P. Yang, Z.H. Khan, J.M. Wu, G. Li and A.R. Kamali, *J. Nanomater.*, **2015**, 371679 (2015); https://doi.org/10.1155/2015/371679.
3. U. Ozgur, D. Hofstetter and H. Morkoc, *Proc. IEEE*, **98**, 1255 (2010); https://doi.org/10.1109/JPROC.2010.2044550.
4. P.R. Solanki, A. Kaushik, V.V. Agrawal and B.D. Malhotra, *NPG Asia Mater.*, **3**, 17 (2011); https://doi.org/10.1038/asiamat.2010.137.
5. A. Janotti and C.G. Van de Walle, *Rep. Prog. Phys.*, **72**, 126501 (2009); https://doi.org/10.1088/0034-4885/72/12/126501.
6. A. Al-Mohammad, R. Darwich, M. Rukiah, S.A. Shaker and M. Kakhia, *Acta Phys. Pol. A*, **125**, 131 (2014); https://doi.org/10.12693/APhysPolA.125.131.
7. W.J.E. Beek, M.M. Wienk and R.A.J. Janssen, *Adv. Mater.*, **16**, 1009 (2004); https://doi.org/10.1002/adma.200306659.
8. S. John, S. Marpu, J. Li, M. Omary, Z. Hu, Y. Fujita and A. Neogi, *J. Nanosci. Nanotechnol.*, **10**, 1707 (2010); https://doi.org/10.1166/jnn.2010.2044.
9. N. Salah, S.S. Habib, Z.H. Khan, A. Memic, A. Azam, E. Alarafaj, N. Zahed and S. Habib, *Int. J. Nanomedicine*, **6**, 863 (2011); https://doi.org/10.2147/IJN.S18267.
10. A.N.P. Madathil, K.A. Vanaja and M.K. Jayaraj, *Proc. SPIE*, 6639, 66390J (2007); https://doi.org/10.1117/12.730364.
11. H.R. Ghorbani, F. Mehr, H. Pazoki and B. Rahmani, *Orient. J. Chem.*, **31**, 1219 (2015); https://doi.org/10.13005/ojc/310281.
12. P.-C. Chou, H.-I. Chen, I.-P. Liu, C.-C. Chen, J.-K. Liou, C.-J. Lai and W.-C. Liu, *IEEE Sens. J.*, **15**, 3759 (2015); https://doi.org/10.1109/JSEN.2015.2391271.
13. S. Sawyer, L. Qin and C. Shing, *Int. J. High Speed Electron. Syst.*, **20**, 183 (2011); https://doi.org/10.1142/S0129156411006519.
14. F.M. Akwia and P. Watts, *Chem. Commun.*, **54**, 13894 (2018); https://doi.org/10.1039/C8CC07427E.
15. E. Neshataeva, T. Kümmell, A. Ebbers and G. Bacher, *Electron. Lett.*, **44**, 1485 (2008); https://doi.org/10.1049/el:20081841.
16. T.V. Kolekar, H.M. Yadav, S.S. Bandgar and P.Y. Deshmukh, *Indian Streams Res. J.*, **1**, 1 (2011).
17. M.A.M. Moazzen, S.M. Borghei and F. Taleshi, *Appl. Nanosci.*, **3**, 295 (2013); https://doi.org/10.1007/s13204-012-0147-z.
18. A. Vanaja and K. Srinivasa Rao, *Int. J. Adv. Mater. Sci. Eng.*, **4**, 1 (2015).
19. M. Gusatti, G.S. Barroso, C.E.M. Campos, D.A.R. Souza, J.A. Rosário, R.B. Lima, C.C. Milioli, L.A. Silva, H.G. Riella and N.C. Kuhnen, *Mater. Res.*, **14**, 264 (2011); https://doi.org/10.1590/S1516-14392011005000035.
20. A.K. Zak, R. Razali, W.H. Abd Majid and M. Darroudi, *Int. J. Nanomed.*, **6**, 1399 (2011); https://doi.org/10.2147/IJN.S19693.
21. R.M. Alwan, Q.A. Kadhim, K.M. Sahan, R.A. Ali, R.J. Mahdi, N.A. Kassim and A.N. Jassim, *Nanosci. Nanotechnol.*, **5**, 1 (2015); https://doi.org/10.5923/j.nn.20150501.01.
22. Z.R. Khan, M. Arif and A. Singh, *Int. Nano Lett.*, **2**, 22 (2012); https://doi.org/10.1186/2228-5326-2-22.
23. P. Bindu and S. Thomas, *J. Theoretical Appl. Phys.*, **8**, 123 (2014); https://doi.org/10.1007/s40094-014-0141-9.
24. A. Arora, S. Devi, V. Jaswal, J. Singh, M. Kinger and V. Gupta, *Orient. J. Chem.*, **30**, 1671 (2014); https://doi.org/10.13005/ojc/300427.
25. J. Mayekar, V. Dhar and S. Radha, *Int. J. Res. Eng. Technol.*, **3**, 43 (2014).